Title

The Electronic Structure of the Mn4Ca Cluster

Authors

Yachandra, VK

Glatzel, P

Yano, J

et al.

Publication Date

2023-12-09

Peer reviewed

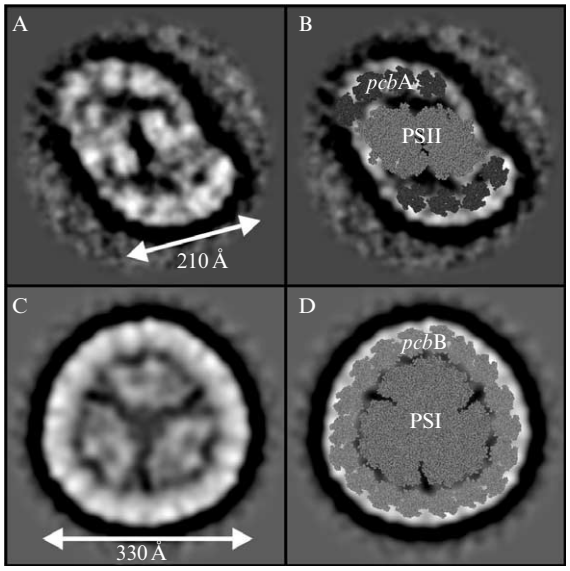

Figure 1: Characteristic top views of negatively stained particles isolated from *Prochlorococcus* MIT9313 cells grown in the presence of iron (A, B) or absence of iron (C, D) as viewed by electron microscopy and shown after overlaying the X-ray structures of a PSI trimer, PSII core dimer and CP43 (as a model for Pcb). The Pcb proteins marked are the products of the *pcb*A (or 0584) or *pcb*B (or 2809) genes respectively (see text).

SDS-PAGE and N-terminal sequencing indicated that the Pcb protein of the PSI supercomplex is derived from the *pcb*B gene. This gene product was readily observed in SDS-PAGE profiles of thylakoid membranes isolated from cells grown under iron deficiency. It ran at a slightly higher apparent molecular mass compared with the PcbA protein observed in both +Fe and −Fe cells consistent with the difference in their predicted molecular masses of 38,511 Da (PcbA) and 40,737 Da (PsbB). The Pcb-PSII supercomplexes observed with iron-supplemented cells were also present in iron deprived cells.

Phylogenetic analyses of the *pcb*/*isi*A/*psb*B/*psb*C gene superfamily (Garczarek et al 2001) indicate that the *pcb*A and *pcb*B genes of MIT 9313 partition into two different clusters and that the latter is very closely related to the *pcb*G gene of *Prochlorococcus* SS120, which is the gene providing the Pcb protein of the 18-mer Pcb-PSI supercomplex of this strain under iron-replete conditions. In the case of MED4 we have been unable to detect an 18-mer *pcb*-PSI supercomplex either under iron-rich or iron-depleted conditions. Indeed in this strain the expression of the single *pcb* gene (*pcb*A) was not significantly effected by iron depletion. In fact using EM and associated image analyses of single particles we found that the Pcb proteins of MED4 associated with PSII in a similar fashion to those of MIT9313.

Therefore we conclude that the PcbA protein of MIT9313 and the PcbA protein of MED4, are targeted to PSII where they interact with the reaction centre dimer and increase the light harvesting capacity of this photosystem. In contrast the PcbB protein of MIT 9313, like the PcbG protein of SS120, is targeted to PSI where it forms an 18-mer light-harvesting antenna ring around the PSI reaction centre trimer. Under iron depletion, expression of the *pcb*C gene of strain SS120 strongly increased while expression of *pcb*G was down-regulated. It is therefore possible that PcbC replaces PcbG in Pcb-PSI supercomplexes under these conditions. The other *pcb* genes of SS120 are probably targeted to PSII.

ACKNOWLEDGMENTS

JB thanks the Biotechnology and Biological Science Research Council for financial support. FP and IM were supported by the EU program "Margenes" (QLRT-2001-01226) and IM was awarded a PhD grant from "Région Bretagne". JN holds a Royal Society University Fellowship.

REFERENCES

Bibby, T. S., Mary, I., Nield, J., Partensky, F. & Barber, J. (2003) *Nature* 424: 1051–1054.

Bibby, T. S., Nield, J., Partensky, F. & Barber, J. (2001a) *Nature* 413: 590.

Bibby, T. S., Nield, J. & Barber, J. (2001b) *Nature* 412: 743–745.

Boekema, E. J., Hiffney, A., Yakushevska, A. E., Piotrowski, M., Keegstra, W., Berry, S., Michel, K.-P., Pistorius, E. K. & Kruip, J. (2001) *Nature* 412: 745–748.

Ferreira, K., Iverson, T., Maghlaoui, K., Barber, J. & Iwata, S. (2004) *Science* 303: 1831–1834.

Garczarek, L., van der Staay, G. W., Hess, W. R., Le Gall, F. & Partensky, F. (2001) *Plant Mol. Biol.* 46: 683–693.

Jordan, P., Fromme, P., Witt, H. T., Klukas, O., Saenger, W. & Kraus, N. (2001) *Nature* 411: 909–917.

La Roche, J., van der Staay, G. W., Partensky, F., Ducret, A., Aebersold, R., Li, R., Golden, S. S., Hiller, R. G., Wrench, P. M. & Larkum, A. W. (1996) *Proc. Natl. Acad. Sci. USA* 93: 15244–15248.

Mary, I. & Vaulot, D. (2003) *FEMS Microbiol. Lett.* 225: 9–14.

Moore, L. R. & Chisholm, S. W. (1999) *Limnol. Oceanogr.* 44: 628–638.

Partensky, F., Hess, H. R. & Vaulot, D. (1999) *Microbiol. Mol. Biol. Revs.* 63: 106–127.

Partensky, F., La Roche, J., Wyman, K. & Falkowski, P. (1997) *Photosynth. Res.* 51: 209–222.

Strauss, N. A. (1994) in: The Molecular Biology of Cyanobacteria (D. A. Bryant, Ed.) pp. 731–750. Kluwer, Dordrecht, The Netherlands.

van Heel, M., Harauz, G. & Orlova, E. V. (1996) *J. Struct. Biol.* 116: 17–24.

THE ELECTRONIC STRUCTURE OF THE MN_4CA CLUSTER

Pieter Glatzel[1,2], Junko Yano[3], Henk Visser[3,4], John H. Robblee[3,4], Kenneth Sauer[3,4], Stephen P. Cramer[1,3], Uwe Bergmann[5], Vittal Yachandra[3]. [1]Department of Applied Science, University of California, Davis, CA, USA. [2]Department of Inorganic Chemistry and Catalysis, Utrecht University, 3584 CA Utrecht, The Netherlands. [3]Melvin Calvin Laboratory, Physical Biosciences Division, Lawrence Berkeley National Laboratory, Berkeley, CA, USA. [4]Department of Chemistry, University of California, Berkeley, CA, USA. [5]Stanford Synchrotron Radiation Laboratory, Stanford University, Stanford, USA

Keywords: oxygen-evolution, Photosystem II, X-ray spectroscopy, manganese

INTRODUCTION

A key question for the understanding of photosynthetic water oxidation is whether the four oxidizing equivalents generated by the reaction center are accumulated on the four Mn ions of the oxygen evolving complex (OEC), or whether a ligand-centered oxidation takes place before the formation and release of molecular oxygen during the S_3 to (S_4) to S_0 transition.

Mn K-edge XANES has been the traditional X-ray spectroscopic method for determining the oxidation states (Yachandra et al 1996). The development of new technologies has made Mn X-ray emission spectroscopy (Messinger et al 2001) and more recently, X-ray resonant Raman spectroscopy or resonant inelastic X-ray scattering spectroscopy (RIXS) possible to use for studying inorganic Mn complexes and the Mn OEC in all the S-states (Glatzel et al 2004). The description of the Mn OEC in the various S-states in terms of the formal oxidation states, although useful, is limited, and it is also important to determine a detailed view of the electronic structure of the Mn cluster.

We have started exploring the technique of RIXS (Kotani & Shin 2001), which is a two photon technique, which has profited from bright synchrotron sources and improved analyzer instrumentation. Here we present the use of high resolution Kα RIXS, where the incident energy is varied across the Mn K-edge (1s to 3d) using hard X-rays, and the crystal monochromator is scanned over the Kα emission energy (2p to 1s). The final state for this transition is identical to that of an L-edge transition where a 2p electron is directly promoted into a 3d level (Fig. 1). The difference compared to a conventional fluorescence-detected K-edge XANES measurement is that the fluorescence is not integrated over the energy range but is detected with high resolution throughout the fluorescence spectrum. As a result, one obtains a two-dimensional contour plot with incident energy along one axis and energy transfer (Raman Stokes shift) along the other axis. The spectral features can be resolved at a high resolution as shown in Fig. 1. Furthermore, this technique offers an unprecedented opportunity to selectively excite into specific molecular orbitals with 3d character by tuning the incoming X-rays to look at a specific pre-edge transition; at least 2–3 resolvable pre-edge transitions are seen in the Mn K-edge spectrum of PS II. The amount of detailed spectral information when compared to the conventional K-edge XANES (black line in Fig. 1) is striking.

MATERIALS AND METHODS

$Mn^{II}(acac)_2(H_2O)_2$ and $Mn^{III}(acac)_3$ were purchased from Alpha products. Mn^{IV}(salicylate)$_2$(bipy) and [Mn^{III}(5-Cl-Salpn)$(CH_3OH)_2$](O_3SCF_3) were provided by the groups of Profs. G. Christou and V. Pecoraro, respectively.

PS II membranes in the S_1 and S_2 states were prepared from spinach and characterized by EPR.

The RIXS data were recorded on the Bio CAT beamline at the APS, Argonne. The scattered X-rays were collected by means of a Ge (3,3,3) crystal array spectrometer. A solid state Ge detector was placed at the common focus of the crystals. Spectra were collected at

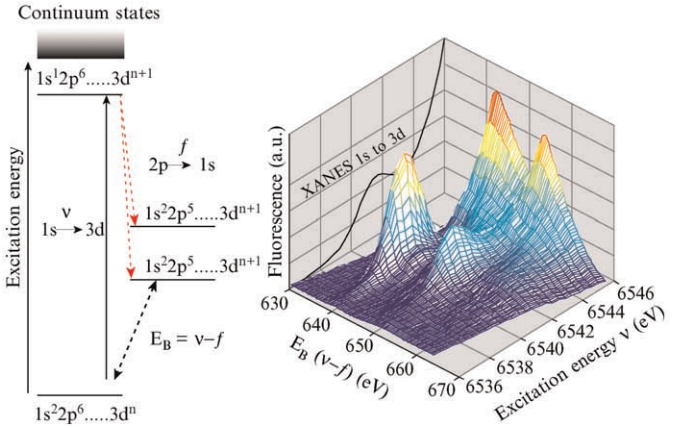

Figure 1: A two-dimensional plot showing the resonant inelastic X-ray spectrum from a Mn(II)acetylacetonate complex. X-axis is the excitation energy across the 1s–3d energy range of the spectrum. The 1s–3d K-edge spectrum is plotted in the back of the 2-dimensional spectrum for reference. Y-axis is the difference between the excitation and emission energy. The deconvolution of the 1s–3d spectrum is significantly better than one can obtain from a simple K-edge spectrum. An integration of the 2D plot parallel to the Y-axis yields L-edge like spectra, the more intense feature at 640 eV corresponds to transitions to J = 3/2 like states (L_3 edges) and transitions at 655 eV correspond to J = 1/2 final states (L_2 edges). Integrations parallel to the energy transfer axis sort the spectrum according to the final state.

10 K. To obtain the two-dimensional RIXS plane we recorded constant emission energy scans with the spectrometer energy changed stepwise. Intensity due to excitations at incident energies higher than the pre-edge was subtracted from the RIXS spectra. RIXS spectroscopy considerably improves the pre-edge extraction because the energy transfer direction is added that separates the pre-edge from the main edge.

Integrations were performed along both the incident energy and energy transfer axis and a first moment analysis of the plots thus obtained was performed to quantify the information contained in the RIXS spectra.

RESULTS AND DISCUSSION

Resonant Raman X-Ray Spectra of Mn Coordination Complexes and PS II. The 1s2p RIXS spectra of three coordination complexes in oxidation states (II), (III) and (IV) as well as the S_1 and S_2 states of PS II are shown in Fig. 2. A striking similarity in the spectral shapes is found between the Mn(II), Mn(III) and Mn(IV) coordination complexes and Mn oxides in oxidation states (II), (III) or (IV) (not shown). The Mn(II) complex shows one pre-edge structure. The structure, however, is less broad indicating a smaller crystal field splitting in the coordination complex. The feature on the high energy transfer side appears more pronounced for the Mn(II) coordination complex than for MnO. This suggests a stronger (2p,3d) final state interaction in case of the molecular complex. It is noteworthy that we obtain identical first moments for MnO and $Mn^{II}(acac)_2(H_2O)_2$ in the incident energy direction but a shift of 0.3 eV to lower energy transfer for the coordination complex compared to the oxide.

We observe a rise of intensity at higher incident energies with increasing oxidation state. Again we observe a rather sharp peak

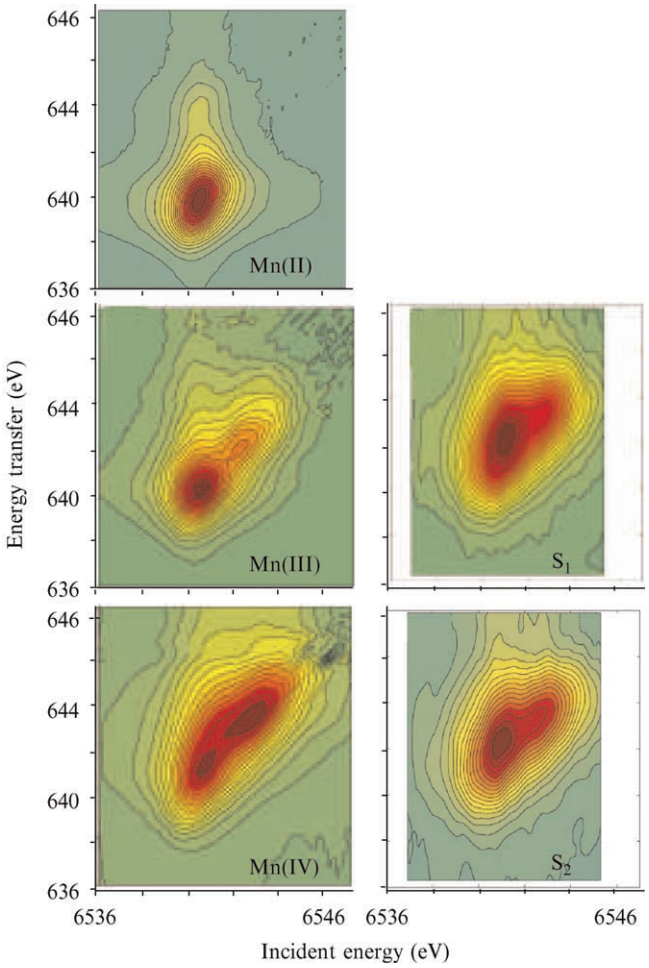

Figure 2: Contour plots of the $1s2p_{3/2}$ RIXS planes for three molecular complexes $Mn^{II}(acac)_2(H_2O)_2$, $Mn^{III}(acac)_3$, and $Mn^{IV}(sal)_2(bipy)$ and PS II in the S_1- and S_2-state. One axis is the excitation energy and the other is the energy transfer axis. The L-edge like spectra are along the energy transfer axis and the 1s to 3d transition is along the excitation energy. The assignment of $Mn(III_2,IV_2)$ for the S_1 state is apparent in these spectra (Glatzel et al 2004).

at low energies and a broad band at high energies. The Mn(IV) coordination complex displays a distinct spectral shape in the contour plot. Unlike all other Mn models with oxidation states higher than II the two structures do not lie on a straight diagonal line but appear bend towards larger energy transfer.

The first moment values increase with the formal oxidation state and the increase is larger in the energy transfer direction.

For the PS II samples the first peak appears broader than for the model compounds and the two structures are not as well separated. The PS II spectra show an average of the four Mn atoms in the tetranuclear cluster that all have a more or less different electronic structure and, as a result, the spectral features become more diffuse. The overall spectral shape, however, is still similar to that of the Mn model systems. The first moments along the incident energy axis for the PS II samples are lower than for the Mn(IV) complex and larger than for Mn(III) in agreement with the proposed oxidation state of $Mn(III_2,IV_2)$ and $Mn(III,IV_3)$ for S_1 and S_2, respectively. The PS II results for first moments on the energy transfer axis match with the Mn(IV) complex.

Like in the model compounds we find that the shift for the energy transfer moment is larger than that for the incident energy. The shifts between S_1 and S_2 are a factor 7–8 smaller than between $Mn^{III}(acac)_3$ and the Mn(III) complex and about a factor 3 smaller between $[Mn^{IV}(5\text{-Cl-Salpn})(CH_3OH)_2](O_3SCF_3)$ and the Mn(IV) complex.

We find that the model systems simulate the correct trends for PS II. When comparing the changes between S_1 and S_2 to the mononuclear model compounds one has to multiply the PS II values by a factor of 4 because one out of four Mn atoms in the OEC is oxidized. The changes between Mn^{III} and Mn^{IV} coordination complexes approximately reproduce the values for S_1 and S_2.

Summary and Conclusions. We have initially focused on the 1s to 3d aspect of the RIXS spectra, where line splittings have been interpreted within a ligand field multiplet model. The results indicate strong covalency for the electronic configuration in the OEC and we conclude that the electron is transferred from a strongly delocalized orbital for the S1 and S2 transition (Glatzel et al 2004). Further RIXS studies that analyze data along the L-edge like 2p to 3d axis are in progress. The energy transfer final states are sensitive to the valence shell spin state via the (2p,3d) multiplet interaction. This will allow for a more detailed analysis and give new information on the (2p,3d) multiplet interactions and thus the Mn spin state.

ACKNOWLEDGMENTS

This research was supported by NIH (GM 55302), and the Director, Office of Science, Office of Basic Energy Sciences, Chemical Sciences, Geosciences, and Biosciences Division of DOE, under Contract DE-AC03-76SF00098. Synchrotron radiation facilities were provided by the SSRL, which is operated by DOE, Office of Basic Energy Sciences. The SSRL Biotechnology Program is supported by NIH, National Center of Research Resources, Biomedical Technology Program, and by DOE, Office of Health and Environmental Research. APS is supported by DOE, Basic Energy Sciences, Office of Science, under contract No. W-31-109-ENG-38. BioCAT is a NIH-supported Research Center RR-08630.

REFERENCES

Kotani, A. & Shin, S. (2001) *Rev. Mod. Phys.* 73: 203–246.

Glatzel, P., Bergmann, U., Yano, J., Visser, H., Robblee, J. H., Gu, W., de Groot, F. M. F., Christou, G., Pecoraro, V. L., Cramer, S. P. & Yachandra, V. K. (2004) *J. Am. Chem. Soc.* 126: 9946–9959.

Messinger, J., Robblee, J. H., Bergmann, U., Fernandez, C., Glatzel, P., Visser, H., Cinco, R. M., McFarlane, K. L., Bellacchio, E., Pizarro, S. A., Cramer, S. P., Sauer, K., Klein, M. P. & Yachandra, V. K. (2001) *J. Am. Chem. Soc.* 123: 7804–7820.

Yachandra, V. K., Sauer, K. & Klein, M. P. (1996) *Chem. Rev.* 96: 2927–2950.